Marine Pollution Bulletin 170 (2021) 112622

Contents lists available at ScienceDirect

Marine Pollution Bulletin

journal homepage: www.elsevier.com/locate/marpolbul

Unravelling spatio-temporal patterns of suspended microplastic concentration in the Natura 2000 Guadalquivir estuary (SW Spain): Observations and model simulations

María Bermúdez [a], César Vilas [b], Rocío Quintana [c], Daniel González-Fernández [c], Andrés Cózar [c], Manuel Díez-Minguito [a,*]

[a] Andalusian Institute for Earth System Research (IISTA), Dept. Structural Mechanics and Hydraulics Engineering, University of Granada, Avenida del Mediterráneo s/n, Edificio CEAMA, Granada E-18006, Spain
[b] Instituto de Investigación y Formación Agraria Pesquera (IFAPA), Centro El Toruño, Camino Tiro de Pichón s/n, El Puerto de Santa María E-11500, Spain
[c] University of Cádiz and European University of the Seas (SEA-EU), Instituto Universitario de Investigación Marina (INMAR), Departamento de Biología, Puerto Real E-11510, Spain

ARTICLE INFO

Keywords:
Plastic pollution
Microplastics
Transport mechanisms
Observations
Idealized model
Estuary

ABSTRACT

Microplastics (MPs) patterns in a weakly-stratified estuary were investigated using a combined approach of observations and modeling. The study was conducted in the Guadalquivir River Estuary, which is of high environmental value, yet significantly altered by human activities. The study aims to contribute to understanding and quantifying the land-ocean transport of MPs. Mean concentrations of MPs in the estuary were 0.041 items m^{-3}, with maximum values up to 0.20 items m^{-3}, in agreement with the range reported in other estuaries. Polyethylene floating MPs were predominant. Relationships between increases in MP concentration and local rainfall events were identified in the middle estuary when there were no significant discharges from the head dam. Modeling results mimicked observations and revealed the effects of tidal straining, density-driven, and river flow-induced circulation on the net transport. Convergence of transports favors the MPs trapping in the vicinity of Doñana National Park, overlapping the location of the Estuarine Turbidity Maximum.

1. Introduction

Estuaries are transitional areas between fluvial and marine environments that provide essential ecosystem services. They are among the most productive of all ecosystems, and their sheltered waters are often referred to as "the cradle of the sea" because of their role as hatcheries and nursery grounds for aquatic fauna (Barbier et al., 2011). Estuaries are, however, highly threatened by human activities. One of these threats is the increased plastic pollution entering these environments, primarily from the rivers and diffuse runoff from the surrounding watersheds. Microplastic (MP) pollution (i.e., from plastic particles below 5 mm) is of particular concern due to its potential risks to human health and wildlife (Wright et al., 2013; Wright and Kelly, 2017).

The study of the distribution and abundance of MPs in water bodies has mostly focused on ocean environments (e.g. Cózar et al., 2014; Cózar et al., 2017). However, about three-quarters of the plastic items reported in the global ocean come from land-based sources (Morales-Caselles et al., 2021). Therefore, estuaries appear as key areas to understand and quantify the land-ocean transport of MPs (e.g. González-Fernández et al., 2021). In recent years, the number of studies in river and estuaries has rapidly increased (e.g. Yonkos et al., 2014; Naidoo et al., 2015; Cohen et al., 2019), although the transport dynamics of riverine MPs remains largely unknown. From 19 to 23 million metric tons, or 11%, of plastic waste generated globally is estimated to enter aquatic ecosystems (Borrelle et al., 2020), most of it via estuaries (Lebreton et al., 2017) following the hydrological pathways through the river catchments (Windsor et al., 2019).

The movement of MP particles within estuaries might be expected to mirror that of sediment particles with hydraulically equivalent physical properties (Kane and Clare, 2019). Given that estuaries act as accumulation areas for sediments, estuarine benthic sediments could constitute an important potential sink for MPs (Simon-Sánchez et al., 2019), preventing a significant portion of MPs generated in river catchments from reaching the sea. Systematic studies of sources, fluxes, accumulation

* Corresponding author.
E-mail address: mdiezm@ugr.es (M. Díez-Minguito).

https://doi.org/10.1016/j.marpolbul.2021.112622
Received 31 January 2021; Received in revised form 2 June 2021; Accepted 7 June 2021
Available online 16 June 2021

zones, and degradation of MPs in transitional waters are needed to shed light on the actual transfer pathways from rivers to the open sea (e.g. Yonkos et al., 2014; Sousa et al., 2021).

Stemming from the analogy with sediment transport, hydrodynamic processes can promote a convergence zone of MPs or Estuarine MP Maxima (EMPM) within the estuary. On the contrary, certain meteorological or oceanographic conditions could increase plastic mobilization (Roebroek et al., 2021) and ultimately flush the MPs out of the estuary towards the open sea. Identifying MP trends and accumulation zones in estuaries in conjunction with the physical drivers of the MPs transport can contribute to implementing effective strategies to prevent plastic waste from reaching the ocean.

Intending to fill these gaps, this research addresses the following objectives:

1. To quantify the concentration, basic properties, and distribution patterns of suspended MPs in a prototype weakly-stratified estuary,
2. To estimate the transport of MPs to determine if the estuary acts as a sink of land-based MPs or a source of MPs to the shelf waters under normal conditions,
3. To unravel the relative influence of the river discharge, tidal straining, the density-driven, and the wind-driven circulation on the MPs distribution.

This investigation is conducted in the Guadalquivir River Estuary (GRE) (Fig. 1). The ecosystem of this estuary is of high environmental value (González-Ortegón et al., 2012; de Carvalho-Souza et al., 2019), yet significantly altered by human activities (Ruiz et al., 2015; Llope, 2017), and contributes greatly to the biological productivity and fisheries of the Gulf of Cadiz (Prieto et al., 2009; de Carvalho-Souza et al., 2019). This transitional environmental system has been classified as an EU Site of Community Interest (SCI) in the Natura 2000 Network, and includes the Doñana National Park in its southwestern part.

To address the first and second research questions, samples of plastic debris from a long-term ecological research program were analyzed. The research program consisted of field campaigns performed in the lower and middle part of the GRE under different runoff, salinity and precipitation conditions. Besides plastic samples, in situ data of turbidity, salinity, temperature, and currents were measured. The third question was addressed by means of an idealized numerical model aimed at assessing the MPs' distribution and gaining basic knowledge about the transport mechanisms controlling their distribution, both vertically and along the estuary.

This work is organized as follows. The study area, field data and numerical model are described Section 2. Section 3 presents and discusses the field observations of MP concentrations, along with the comparison between observations and model output, and sensitivity analysis results. Finally, in Section 4, the most important conclusions of the work are provided.

2. Study area and methods

2.1. The Guadalquivir River Estuary

The Guadalquivir river in the SW Iberian Peninsula flows into the Gulf of Cadiz (Atlantic Ocean) forming the GRE, a L_E=110 km long estuary with an average depth of 7 m and widths ranging from 150 at its upstream limit to 800 m downstream (Fig. 1). The GRE is a narrow, tidally-energetic estuary that exhibits a mesotidal range (~3.5 m at spring tides) with the M2 as the dominant tidal constituent (Díez-Minguito et al., 2012). The GRE watershed has mainly a Mediterranean climate, with heavy precipitation events that can occur during the humid period (Oct–Apr). However, the river flows are highly regulated by a series of dams. The most downstream dam (The Alcalá del Río dam) controls the river discharge to the GRE, representing 80% of the total freshwater inputs to the estuary. Discharges are normally below 40 m^3s^{-1} (low river flow conditions), although they can exceed 400 m^3s^{-1} during high river flow conditions in which inflows exceed the storage capacity of the network of reservoirs. The salinity decreases from the sea towards the head of the estuary due to freshwater input; the null point is usually located around 80 km from the estuary mouth. During low river flow conditions, the estuary is weakly stratified, which is evidenced by low values of bottom-surface salinity difference and potential energy anomaly (Díez-Minguito et al., 2013; Cobos et al., 2020).

The GRE constitutes a high biodiversity valuable ecosystem, which has been recognized as a key nursery area for many marine fish and crustacean species –some of them of socio-economical value–, and whose food web is supported by a rich suspended particulate organic matter standing stock (Cañavate et al., 2019; Cañavate et al., 2021). The estuary greatly contributes to the biological productivity and fisheries of the Gulf of Cadiz (e.g. Prieto et al., 2009; de Carvalho-Souza et al., 2019). In fact, the lower stretches of the GRE and the renowned Doñana National Park, which lies at the southwestern margin of the estuary, are part of the Natura 2000 Network.

However, the GRE has been subject to increased anthropogenic pressures derived from land reclamation, dredging, fishing, river regulation, and other activities that have altered its natural balance since the 18th century (Ruiz et al., 2015; Llope, 2017). Urban and agricultural development have contributed to wetland loss, transforming more than 80% of the original marsh surface area, and produced major morphological changes in the estuary. The river flow is highly regulated by 57 dams; Alcalá del Río dam being the closest one to the estuary. This has resulted in a decrease in freshwater inputs to the estuary of around 60% in the last decades, as well as changes in the seasonal patterns of

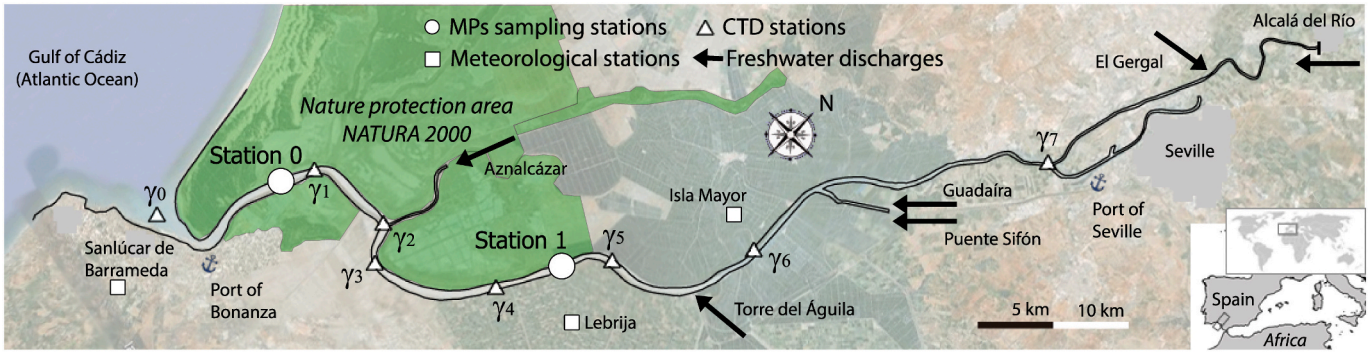

Fig. 1. Study area with the location of the MP sampling sites (circles; Stations 0 and 1), meteorological stations (squares), the main freshwater inflows to the GRE (black arrows) including that from Alcalá del Río dam, CTD stations from where salinity gradient is estimated (triangles) and Nature protection area Natura 2000 (green shaded areas; Doñana National and Natural Park). (For interpretation of the references to color in this figure legend, the reader is referred to the web version of this article.)

discharges, which impacts the aquatic macrofauna (González-Ortegón et al., 2012, 2015). The hyper-turbid conditions and the high nutrient loadings from the surrounding agricultural lands and urban areas, which host approximately 1.7 million people, are also of concern. Highly turbidity levels (Díez-Minguito et al., 2014) yield reduced primary production rates because of light's attenuation by the high suspended sediment concentration (SSC) (Ruiz et al., 2017).

In recent years, further environmental concerns regarding the presence of MPs in the Gulf of Cádiz and the GRE have been raised. The analysis of water quality performed by López-López et al. (2011) identified the city of Seville, with five wastewater treatment plants discharging 250000 m^3d^{-1} into the estuary, the tributary river Guadaira, and the agricultural activities carried out in the middle part of the GRE as the main pollution inputs. Nevertheless, pollution due to MPs was not considered in this study. However, it is worth noting that first assessments of the abundance of MPs in the Gulf of Cádiz pointed to the Guadalquivir River as the greatest contributor of MPs (Quintana et al., 2020) and suggested to focus future monitoring efforts in this area (González-Ortegón et al., 2020).

2.2. Field data

Samples of plastic debris were collected on a lunar monthly basis from January 2014 to December 2015 to analyze their properties and abundance. Two sampling sites, located at 8 and 32 km from the estuary mouth, respectively, were chosen (Station 0 and Station 1; circles in Fig. 1). Samples were taken during spring tides from a boat anchored to the bottom and equipped with three large nets separated from the boat that sampled in parallel along each cross-section. Each of these three nets, which were 20 m in length, had a mesh size of 1 mm and a mouth opening of 2.5 m (width) × 3 m (depth). During each spring tide sampling period, a total of 4 passive trawl fishing samples were taken at each station, 2 during the maximum flood tide and 2 during the maximum ebb tide, covering a 24-h tidal cycle. Water velocities were measured with Hydrobios flowmeters to estimate the water volume filtered by each net. Total filtered water volume was around (58000 ± 23000) m^3 per sample. A total of 200 samples were analyzed in this work.

In the laboratory, MP particles were separated according to their size using a sieve. The samples were transferred into Petri dishes, and potential MPs were separated from zooplankton and organic tissues and carefully picked out with the aid of a dissecting stereo microscope. Samples were double-checked to ensure the detection of all potential plastic particles, even the smallest and/or transparent plastic particles. Once this step was completed, Fourier Transform Infra-Red (FTIR) spectroscopy analyses on a subset of potential MPs confirmed the plastic nature of 94.3% of the particles. Plastic items were classified according to shape/origin in six types: raw industrial pellets, microbeads (likely derived from cosmetic and cleansing products), films (mostly derived from discarded bags and packings), foamed plastic, rigid (thick-walled) fragments, and lines (Martí et al., 2020) (likely derived from nets and fishing lines). Fibers (sensu Cózar et al. (2015)) were excluded from the analysis because they were probably underrepresented in the samples taken by a net with 1 mm pore size.

Along-channel density gradients were obtained from CTD data recorded from 2008 to 2011 in eight environmental sampling stations installed along the *thalweg* (Navarro et al., 2011). These devices (marked as triangles, and denoted as γ_k in Fig. 1) measured conductivity, turbidity, and temperature every 30 min (during some periods every 15 min). Station γ_0, the seamost sampling station, was selected as the origin of the along-channel coordinate x, which is taken to represent positive landward direction.

Hydrological and meteorological data during the MPs sampling were obtained from available databases from public agencies. Daily discharge records at Alcalá del Río (gauging station code 5072), and other minors tributaries, namely, El Gergal (5042), Guadaira (5057), Puente Sifón (5132), Torre del Águila (5022), and Aznalcázar (5076), were provided by the monitoring network of the Regional Water Management Agency (Red de seguimiento de la Confederación Hidrográfica del Guadalquivir, MAPAMA). Discharge inputs into the estuary from these streams are indicated in Fig. 1 with black arrows. Wind velocity and direction and rainfall data were obtained from meteorological stations maintained by the Instituto de Investigación y Formación Agraria y Pesquera (IFAPA) (Red de Información Agroclimática - Regional Government - Junta de Andalucía). In particular, data from stations Isla Mayor, Lebrija, and Sanlúcar de Barrameda were used. These stations are marked in Fig. 1 as squares.

2.3. Numerical model

A tidally-averaged 2D exploratory model is implemented to analyze longitudinal transport mechanisms and spatial distribution patterns of MPs in the GRE. A similar approach was considered to model MP transport in the coastal upwelling system of the Ría de Vigo, Spain (Díez-Minguito et al., 2020). The idealized model was originally inspired by that of Talke et al. (2009), but adapted and extended to study MP transport. The reader is referred to Supplement A for additional details on the model and its implementation. Only a brief description of its main features and set-up is given here.

The model assumes stationary conditions at a tidally-averaged scale to estimate longitudinal currents $\langle u(x,z)\rangle$, with $0 \le x \le L_E$ and $-H(x) \le z \le 0$ the longitudinal and vertical coordinates, respectively. The net circulation $\langle u\rangle$ includes the contribution due to the river, density-driven flow, wind-induced flow, and tidal straining (e.g. Burchard and Hetland, 2010). Other processes such as tidal pumping, which could be relevant in transporting suspended matter (Díez-Minguito et al., 2014), are not included in the model. The model is thus forced with a given freshwater discharge Q at the landward boundary. The along-estuary salinity gradient and wind profile are prescribed and indicated in Table 1. Typical salinity and wind profiles are sketched in Fig. 2 along with the bathymetry details implemented for the GRE. The correlation between the fluctuating part of the eddy viscosity and the vertical shear of velocity, which drives the estuarine circulation due to tidal straining, is also prescribed (Table 1).

Microplastics are modeled as passively transported by the water flow and dispersed by turbulent mixing, and are characterized by a terminal (rising) velocity, ω_{MP} (e.g. Waldschläger et al., 2020). The vertical distribution of tidally-averaged MP concentration (MPC) is obtained imposing that the vertical flux of MPs is balanced by turbulent mixing (Talke et al., 2009). Tidally-averaged eddy viscosity and diffusivity coefficients are defined as A_{v0} and K_{v0}, respectively. The model neglects density stratification, which seems appropriate for the GRE, which is mostly a weakly-stratified estuary. The dependence of eddy coefficients on the Richardson number is thus ignored, and, according to Bowden et al. (1959), $A_{v0} \approx K_{v0}$ is assumed.

2.3.1. Design of experiments

Three series of experiments are designed to explore the behavior of suspended MPs in the GRE. All experiments are performed using the depth and width profiles shown in Fig. 2. The grid of the model is 300 × 100 cells in the along-channel and the vertical direction.

The first series of experiments aims to verify the ability of the idealized model to capture some of the observed features of the MPC in the GRE (Section 3.2.1). Modeled MPC was compared with the observed values at the same conditions that occurred during the field campaign. The relative importance of the freshwater discharge, wind-driven, density-driven, and tidal straining transports is quantified.

Regarding the drivers of the estuarine circulation, the value of the freshwater discharge is set to Q=15 m^3s^{-1}, which is approximately the mean value during the field campaign period at low flow conditions. The salinity gradient driving the density-driven circulation is determined by fitting a typical tanh profile with a fixed value of salinity at the shelf of S_0=35.5 psu (Table 1) to along-channel salinity distributions observed at

Table 1
Along-channel salinity, $S(x)$, and wind, $w(x)$ and fluctuating part of the eddy viscosity, A_{v0}'. Goodness of the fits are quantified in terms of the Squared 2-norm of the residuals. (Additional information in Supplement A.)

	Formulae	Parameters	Residuals
S (psu)	$S_0\left(1-tanh\left(\frac{x-x_c}{x_L}\right)\right)$ $x_c = aQ^{-b}$, $x_L = cQ^{-d}$	S_0=35.5 psu a=40.8, b=0.42 c=50.61, d=0.35	R^2=0.96
w (ms^{-1})	$W_0 e^{-\left(\frac{x}{L_0}\right)^2}$	W_0=2.52 ms^{-1}, L_0=4 · 10^{2}km	R^2=0.47
A_v' (m^{2}s^{-1})	$A_{v0}' e^{-\left(\frac{x-x_{ca}}{x_{La}}\right)^2}$	A_{v0}'=0.19 m^{2}s^{-1}, x_{ca}=25 km, x_{La}=10 km	R^2=0.63

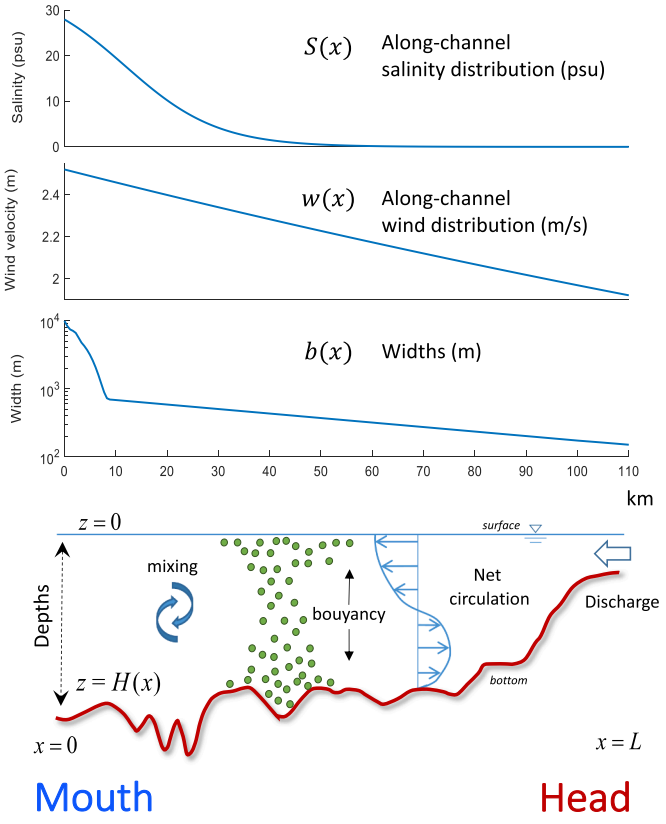

Fig. 2. Sketch of the model geometry (depth and width) showing model forcings and (hypothetical) net circulation within the estuary (along-channel distribution of forcings are given in Table 1). Particle buoyancy and turbulent mixing, as important processes included in the modeling, are also schematized.

the CTD stations (Fig. 1) for different river flows. Wind velocity along the estuary is modeled using a decreasing stretched exponential profile from the mouth to the head (Table 1). The velocity value at the mouth, W_0, and the e-folding scale, L_0, are set using meteorological observations from the Lebrija, Sanlúcar and Isla Mayor meteorological stations (Fig. 1).

Using typical hydraulic parameter values in the GRE (Díez-Minguito et al., 2012), the tidally-averaged eddy coefficients are estimated as $A_{v0} \approx K_{v0} \approx 0.0123\,m^2s^{-1}$, which is within the typical range estimated by Reyes-Merlo et al. (2013) for the lower part of the GRE (see Supplement A). The along-channel dependence of the fluctuating part of the eddy viscosity (A_v') is assumed to be gaussian-like centered in the lower third of the estuary (Table 1), where tidal straining is recognized to be relevant (Díez-Minguito and de Swart, 2018; Cobos et al., 2020). The order of magnitude of the correlation between A_{v0}' and the vertical shear of velocity ($\partial u'/\partial z$) is firstly estimated from observations of vertical profiles of longitudinal current and salinity (Navarro et al., 2011). Then, A_{v0}' was refined to mimic closely the observed mean MPC values during the field campaign. Best results are obtained for $A_{v0}'/A_{v0} \approx 15.5$.

Waldschläger et al. (2020) provide estimates of effective terminal velocities from environmental MP samples. As will be presented in Section 3.1, the most abundant MP type found in the GRE was polyethylene film-type MPs with positive buoyancy. Most sizes were from 1 mm to 5 mm. Following Waldschläger et al. (2020), a rising velocity of ω_{MP}=0.0046 ms^{-1}, which maps into a bulk density of 0.98 gcm^{-3} and equivalent particle diameter of 2.3 mm, is chosen as representative of this type. Simulations performed using this value, along with those of the turbulent coefficients, mimicked closely the observed MPC at Stations 0 and 1 without any further fitting (see results in Section 3.2.1).

Once the model was verified, a second and third series of experiments are performed to test the sensitivity of the MPs distribution patterns to freshwater discharge and to different types or sizes of MP (Section 3.2.2). The second series of experiments explores the response of the MPs distribution patterns to different freshwater discharges, and thus to salinity gradients, too. The terminal velocity of MP particles is kept constant, with the same value to that in the first series of experiments. Freshwater discharges between 1 m^{3}s^{-1} and 150 m^{3}s^{-1}, i.e., below the threshold of high river flow conditions (Q<400 m^{3}s^{-1}) (Díez-Minguito et al., 2012), are considered. The along-channel salinity distribution changes depending on the particular value of the freshwater discharge, as is indicated in Table 1.

The third series of experiments explores the MPs distribution variability regarding different types of MP. With this aim, different rising velocities are considered ranging from ω_{MP}=0.001 ms^{-1} to ω_{MP}=0.010 ms^{-1}. This interval comprises the range of values determined by Waldschläger et al. (2020) for floating polyethylene film-type MPs. Following these authors (Supporting Information), these velocities approximately correspond to MP bulk densities between 0.600 gcm^{-3} and 0.983 gcm^{-3} or equivalent particle diameters between 1.0 mm and 3.7 mm. The salinity gradient and wind profiles, freshwater discharge and turbulent parameters are kept as in the first series of experiments.

3. Results and discussion

3.1. Observations

A total of 19,371 plastic items were collected in the monitoring of the GRE. Microplastics (defined here as plastic items from 1 mm and 5 mm) accounted for the 60.8% of the total plastic items sampled. They were made of polyethylene (87%), polypropylene (12%), and polyamide (1%). The highest percentage corresponded to films (70.1%), followed by fragments (25.3%) and fishing lines (4.5%). There were practically no foam or pellets found in the samples. This composition of MPs per morpho-types is consistent with the observations made in other estuaries around the world. In five estuaries along the Durban coastline (South Africa), film-types and rigid fragments comprised the largest proportion of all plastic items found in the surface water, representing more than 80% in the most populated estuary (i.e., Durban Bay estuary) (Naidoo et al., 2015). Several studies in estuaries of the United States found a marked occurrence of fragments in intertidal sediments (Gray et al.,

2018) and in surface waters (Cohen et al., 2019), particularly in samples taken at urban/suburban watersheds (Yonkos et al., 2014). Since there was no film category in these studies, film-type and rigid fragments were presumably both classified as fragments.

Fig. 3 shows the time series of average MPC at Station 0 and 1 (panels a and b), freshwater discharge (panel c and inset c1), rainfall (panel d), and wind data speed (panels e and d). Average MPC at Stations 0 and 1 (panels a and b) were very similar, viz. 0.0416 items m^{-3} and 0.0415 items m^{-3}, respectively. Maximum values of 0.15 items m^{-3} and 0.20 items m^{-3} were attained at Stations 0 and 1, respectively. The net mesh size of 1 mm used in this study may provide much lower concentrations than those described in studies with smaller mesh sizes (Lindeque et al., 2020). Still, peak MP concentrations in the GRE are comparable to those observed in other estuarine areas. Simon-Sánchez et al. (2019) measured MPCs as high as 3.5 items m^{-3} in surface waters of the Ebro River Delta. In the Delaware Bay, Cohen et al. (2019) observed baywide values ranging from 0.19 items m^{-3} to 1.24 items m^{-3}. Prata et al. (2021) reported values on the same order of magnitude in the Douro River Estuary, viz. 0.23 items m^{-3}. A significant river flow-induced variability of MP concentrations between 0.005 and 0.7 items m^{-3} was found by Mai et al. (2019) in the Pearl River Delta.

The patchiness associated with plastic pollution, together with the inherent space-time variability of the environmental drivers, hinders the interpretation of the field campaign results, particularly with regard to finding correlations between the measured MP concentrations and the physical forcings. The search for a straightforward relationship between MPC and discharges released by the upstream dam, as occurs in other estuaries (e.g. Mai et al., 2019), was inconclusive (Fig. 3, panel c). At Station 0, the closest to the estuary mouth, the highest MPCs do not seem to be associated with high river flows. At Station 1, MPCs are relatively constant during the study period, and do not appear to change substantially in response to high flows. However, it should be noted that the sampling was limited to two sites and mostly performed during low-flows. High discharge values are thus under-represented in the field data. Nevertheless, these limitations of the field campaign can be overcome by numerical modeling experiments, as will be shown in Section 3.2. Flows from smaller streams could be a relevant source of MP pollution in the estuary (inset c1 in panel c). They represent less than 20% of the total freshwater inputs to the estuary and tend to follow the same temporal pattern as the discharges from Alcala del Río. The only exception is that of Salado de Morón stream (gauging station of Torre de Águila), which flows into the estuary at a location close to the sampling Station 1. Inflows from this stream could explain, for example, the higher concentrations recorded at Station 1 on July 2014, which equaled those at Station 0, with low flows from Alcalá del Río.

Stormwater runoff that discharges directly into the estuary during local rainfall events (Fig. 3, panel d) could yield local changes in MPCs. In fact, the relation between local precipitation events and relative increases in MPCs at the innermost Station 1 (panel a) is apparently more evident. This could be the case of rainfall events occurred on Dec 25th 2013, Apr 20th 2014, May 21st 2014, Jun 24th 2014, Oct 11th 2015, Jan 19th 2015, and Oct 18th 2015 (identified by vertical boxes in Fig. 3). These events were not linked to high discharges from the Alcalá del Río head dam. MP emissions associated with the latter are likely caused by storm passage events over the whole catchment, i.e., not by local rainfall events. Events with high river flows (e.g., Feb 9th 2014 and Nov 28th 2014) do not seem to show increases in MPC at any of the two stations. On the contrary, as is shown in Fig. 4 (panels a1 and a2), the MPC seems to decrease with increasing freshwater discharges, similarly as salinity does (panels b1 and b2), at both stations. This behavior could be explained by the seaward advection of MPs beyond Station 0 induced by high river flows from the Alcalá del Río dam. The data dispersion is high, and a straightforward empirical relationship cannot be inferred from the observations in this period, though.

Linkages between discharge, MPC and SSC have been reported in other estuaries (e.g. Cohen et al., 2019), in spite of the high variability of

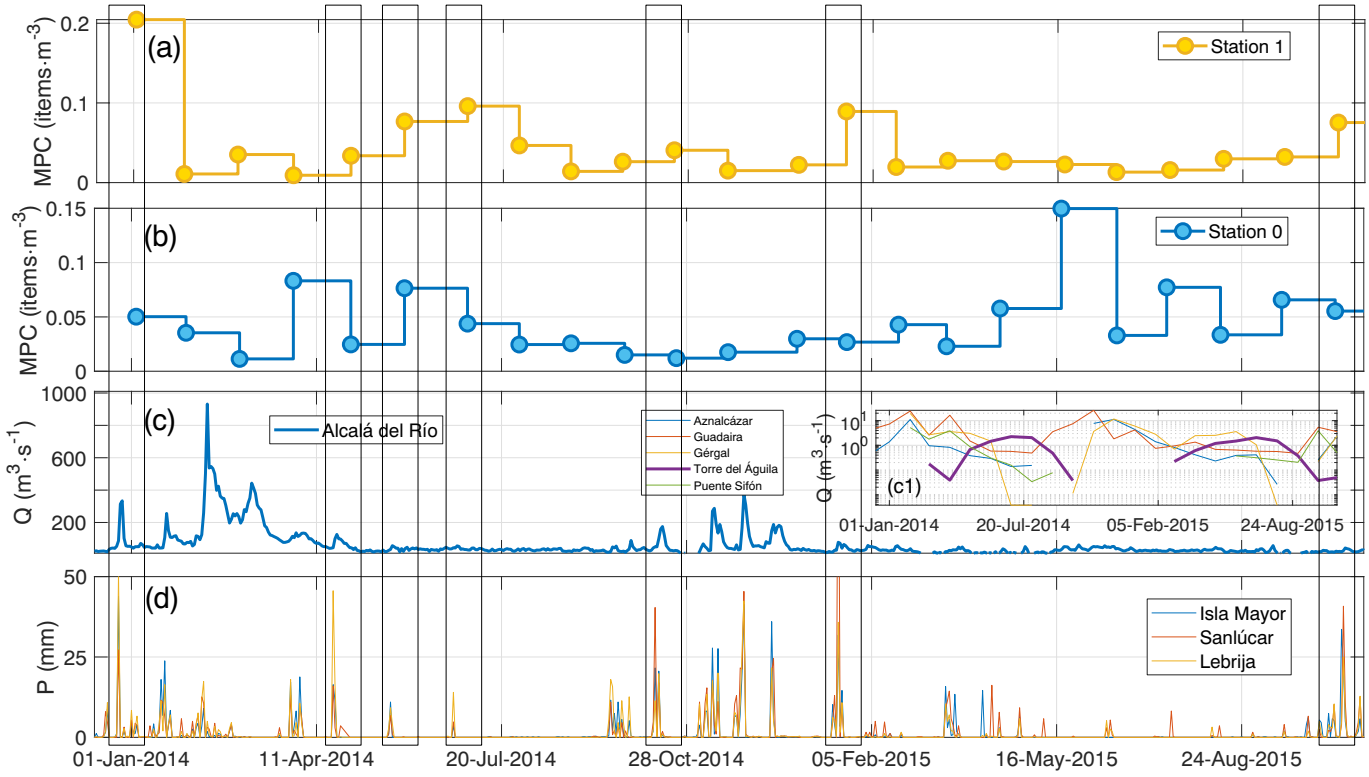

Fig. 3. Time series during the field campaign period of mean microplastic concentration at Station 1 (panel a) and Station 0 (panel b), freshwater discharges into the estuary from Alcalá del Río dam (panel c) and other smaller streams (inset panel c1), and rainfall recorded at three stations in the study area (panel d). Vertical boxes are to guide the eye to rainfall events and their possible relationships with MPC and *Q*.

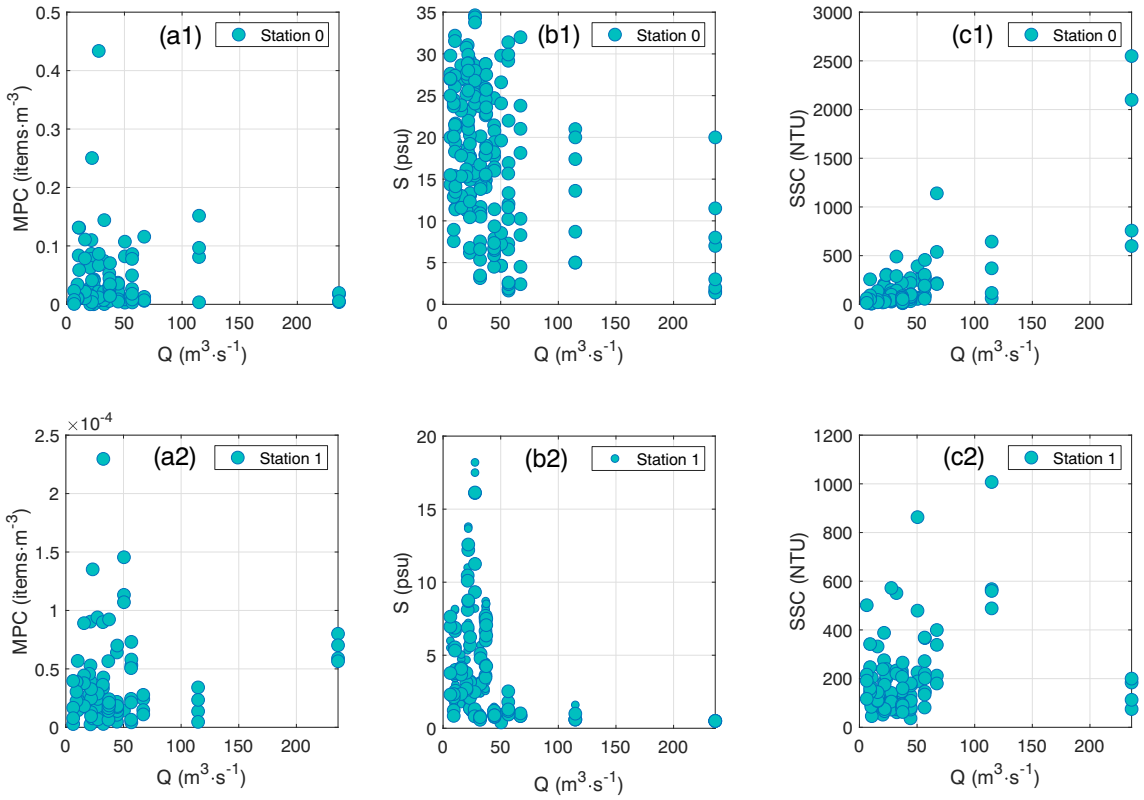

Fig. 4. Scatter plots of microplastic concentration (MPC), salinity (*S*), and suspended sediment concentration (SSC) vs. freshwater discharge (first, second and third column of panels, respectively) at Station 0 (upper row of panels) and Station 1 (lower row of panels).

MP distributions. Values of SSC at Station 0 seem to increase with higher discharges (Fig. 4, panel c1). The concentration of MPs, however, does not increase with higher *Q*, as discussed above. The highest MP concentrations at this station were found under low turbidity conditions. At Station 1, SSC values are lower than those recorded in Station 0 (Fig. 4, panel c2) because the Estuarine Turbidity Maximum (ETM) is located near but downstream Station 1 (Caballero et al., 2014; Díez-Minguito et al., 2014). The highest discharges are not associated with high turbidity levels and MPCs under high flows are in the range of those measured under average conditions.

Due to the large diversity of product types that MPs come from, it is extremely difficult to trace them back to their source (Rochman et al., 2019). Nevertheless, features like size, color, chemical composition, or shape can provide clues of the product they came from and how and where they entered the estuary. Acknowledging the above difficulties, the results presented above may shed some light on the possible origin of plastic debris in the GRE. The predominance of film-type MP (probably largely derived from bags and flexible packaging) may be related to the urban activity and the intense agricultural activity developed Guadalquivir River catchment and the margins of the estuary (Ruiz et al., 2015), with plastic sheeting covering nearly 8000 ha in the Doñana area (WWF, 2019). Microplastic particles can be buried in agricultural soils through the degradation of plastic materials used by farmers (plastic greenhouses, mulches, etc.) or the application of sewage sludge or biowaste composts for fertilization (Weithmann et al., 2018), among others. Even in study sites where microplastic-containing fertilizers and agricultural plastic applications have never been used, a high proportion of film-type MPs can be found (Piehl et al., 2018), which can then be washed down and transferred to the streams and rivers. Diffuse water inputs from the margins could explain the increases in MPC values after local rainfall events, similarly as could occur in beaches (Ryan and Perold, 2021). In any case, further research is needed to identify whether the above sources of MPs are indeed the dominant ones in the GRE.

3.2. Modeling

3.2.1. Default experiment. Field campaign conditions

Fig. 5 shows the net estuarine circulation (panel a) and the distribution of MPs throughout the estuary (panel b and inset b1) during the field campaign period and mean conditions of river flow. Panel c shows the net MP transport and its decomposition into transports induced by density gradient, freshwater discharges, tidal straining, and wind. River flow-induced circulation dominates in the upper and middle estuary (x>40 km), as shown by the unidirectional residual seaward flow in the whole water column (panel a) in the upper and middle estuary. The density-driven flow takes over the control of the circulation near the estuary mouth (x<10 km), thereby inducing a two-layered circulation with seaward flow near the surface and landward compensating flow near the bottom, i.e., as the classical gravitational estuarine circulation. Between km 10 and 40, despite the density-driven flow being larger due to larger salinity gradients, the circulation is dominated by the tidal straining contribution, which apparently opposes the gravitational circulation. The effect of local winds in the modeled net circulation represents the lowest contribution, except perhaps near the mouth, where the estuary opens to the sea. Thus, overall, the dominant mechanisms driving the net circulation (panel a) depend on the location within the estuary, being the tidal straining, the density-driven, and the river flow-induced circulation the most significant contributions. This is also evidenced by the MP transports (panel c). The net transport (black line) is mostly comprised by the contribution of these three mechanisms. Oscillations in the transports are related to changes in bathymetry, in particular due to the presence of sections of greater average depth, which are typically associated with meanders of high curvature (Fig. 1).

The distribution of MPC (Fig. 5, panel b) shows that most of the material is concentrated in the lower part of the estuary, in the vicinity

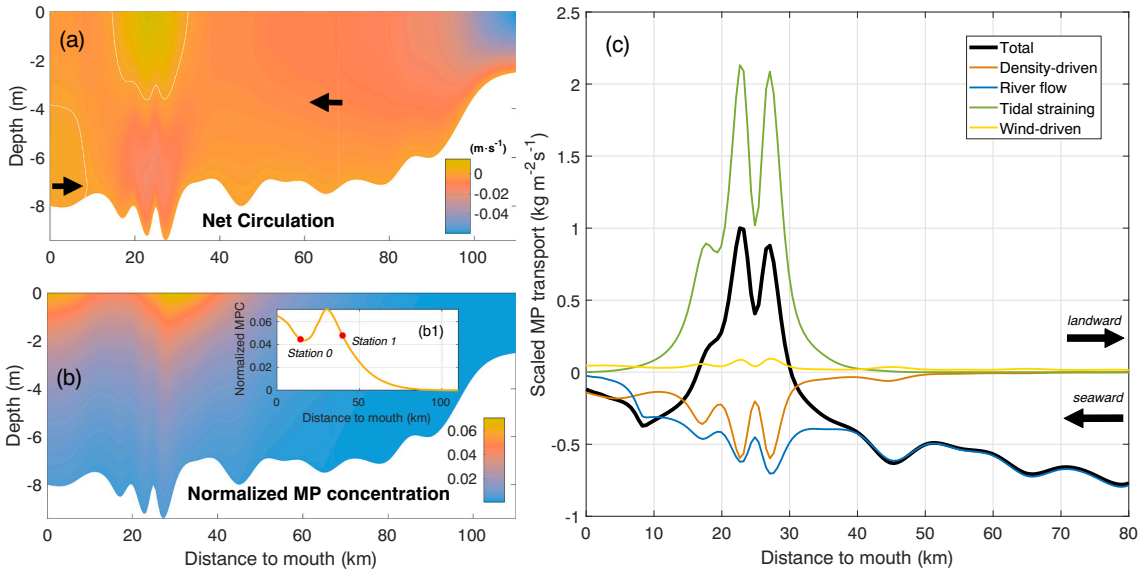

Fig. 5. Left: color plots of net circulation (panel a) and normalized MPC (panel b) for a typical configuration during the field campaign period during mean conditions of river flows. Forcing parameters were set as indicated in Table 1 and ω_{MP}=0.0046 m s^{-1}. Black arrows in panel a show the flow direction areas, which are separated by the white line that indicates the zero-flow isoline. The inset b1 shows the along-channel depth-averaged concentration (solid curve), highlighting the locations of Station 0 and Station 1 (red circles). Panel c shows the net transport of MPs (black curve), which is comprised by the superposition of the density-driven (red curve), river flow (blue curve), tidal straining (green curve), and wind-induced transports (yellow curve). Black arrows indicate the transport direction. (For interpretation of the references to color in this figure legend, the reader is referred to the web version of this article.)

of the Doñana National Park - Red Natura 2000 protection area and, to a less extent, near the mouth (Fig. 1). These locations, referred to as primary (the largest one) and secondary Estuarine MP Maxima (EMPM), coincide approximately with the locations of the null-flow isolines (panel a), i.e., where the flow changes its sign. The convergence of MP transports, which is more significant around km 25, yields the trapping of MPs. The primary EMPM is located between sampling Stations 0 and 1, as is shown by the along-channel depth-averaged concentration (inset b1). Modeled depth-averaged (normalized) concentrations at sampling Stations 0 and 1 show a fair agreement with the observed mean MPCs, which verifies the model performance. The ratio between observed average MPC at Stations 1 and 0 was 1.0024 (see Section 3.1), whereas modeled values (circles, inset b1) attain a ratio of 1.0325. The primary EMPM almost happens to coincide with the location of one of the Estuarine Turbidity Maxima (ETM) of the GRE (Caballero et al., 2014; Díez-Minguito et al., 2014). This seems to be a common feature in many estuaries (e.g. Cohen et al., 2019), since MPs are subjected to similar physical transport processes as other suspended particulate matter (Chubarenko et al., 2018).

Regarding the distribution of MPs in the water column, the highest concentrations are exhibited at the near-surface. However, non-zero concentrations are obtained throughout the whole water column due to turbulent tidal mixing, which is quite intense in the tidally-energetic GRE. A straightforward estimate of the Shields' critical stress indicates that tidal currents in the GRE are sufficient even to entrain sinking MPs into the flow and diffuse them throughout the water column (Chubarenko et al., 2018). Indeed, a Shields' critical shear value greater than 1 is obtained, which is sufficient to put MPs in suspension, considering items of diameter 5 mm with relative density excess equal to $\Delta\rho/\rho$=0.03, and typical hydrological values near the EMPM location of water densities ($\rho \sim 1015\,\mathrm{kg\,m^{-3}}$) and tidal current amplitudes (on the order of magnitude of 1 m s^{-1}).

Since the GRE is a relatively narrow estuary, some of the suspended material is expected to be stranded in the intertidal zones (e.g., Gray et al., 2018) due to different processes, such as windage or lateral circulation. These processes, and in particular the beaching of MPs, are not included in the exploratory model. Plastic materials in intertidal zones could significantly affect the growth of plant species in saltmarsh edges and benthic communities that proliferate in the Natura 2000 protection area. Recent investigations point to microphytobenthos as an important support for biological productivity (Díez-Minguito and de Swart, 2020; Miró et al., 2020) in an estuary whose productivity is already impaired by reduced water quality (Ruiz et al., 2017). These environmental risks deserve attention in future research, which could involve the inventory and analysis of stranded plastics in intertidal areas and the development of more complex (lagrangian) models (e.g. Jalón-Rojas et al., 2019) that capture these processes and their control over physical-biotic interactions.

3.2.2. *Sensitivity to river flow and terminal velocity*

Fig. 6 shows the results of the second series of experiments on the sensitivity of the (depth-averaged) MPC distribution to different freshwater discharges (main graph, panel a). The along-channel salinity gradient (panel a1), which drives the density-driven circulation, also varies in response to variations in freshwater discharge according to the expressions indicated in Table 1. Suspended MPs appear to be mostly concentrated around km 35 when discharges are exceptionally low, i.e., below 10 m^{3}s^{-1} (panel a). These low values of Q yield smoother salinity gradients (panel a1). This effect induces in turn a weak density-driven circulation and promotes a larger saline intrusion within the estuary (panel a1). Higher freshwater discharges increase the river flow towards the mouth, thereby enhancing the seaward MP transport. For example, the formation of primary and secondary EMPM around km 30 and near the mouth (discussed in Section 3.1), respectively, becomes evident already for Q=15 m^{3}s^{-1}. In addition, higher freshwater discharges advect the salinity distribution and saline intrusion downstream, thereby increasing the salinity gradient near the mouth while reducing it elsewhere (panel a1). Discharges above ~20 m^{3}s^{-1} yield a significant seaward shift of the primary EMPM, thereby changing the primary-secondary character of the EMPM. For discharges above 60 m^{3}s^{-1}, most of the floating plastic debris seems to be flushed out the estuary.

The response of both EMPM to different river flows is examined in detail in panels a2 and a3, which show concentration values at the EMPM and their locations, respectively, as a function of the discharge. Primary and secondary EMPM apparently coexist below 20 m^{3}s^{-1}. The MP concentration at both EMPM shows a relative increase with

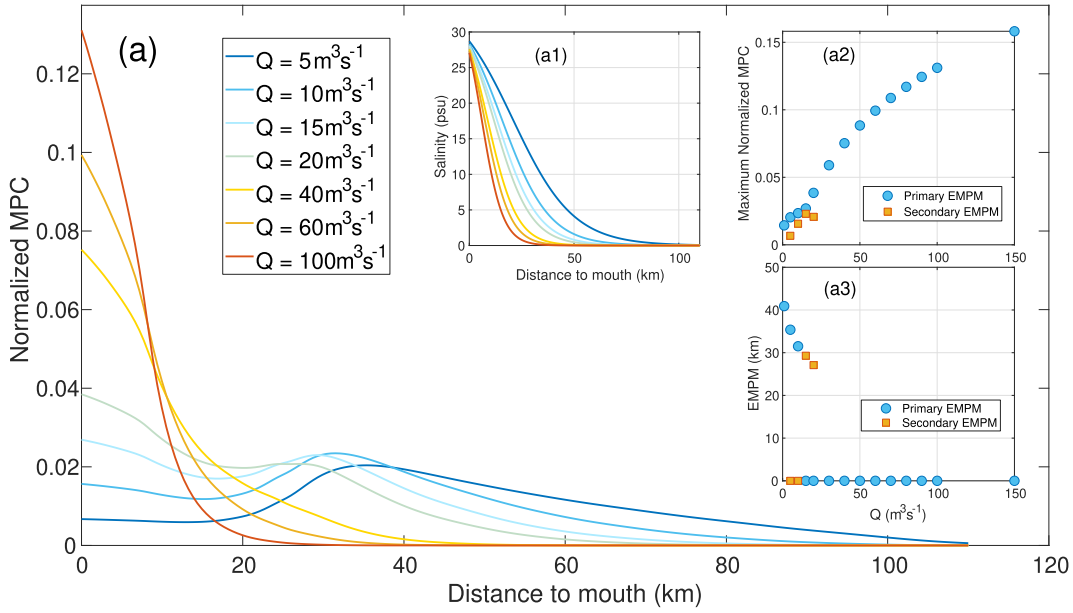

Fig. 6. The main graph (panel a) shows depth-averaged normalized MPC along the main channel of the estuary for different freshwater discharges (legend). Panel a1 shows the corresponding salinity distributions to freshwater discharges (same legend). Panels a2 and a3 show the depth-averaged MPC at the EMPM and the EMPM location as a function of the freshwater discharge, respectively. Blue circles and orange squares stand for primary and secondary EMPM values, respectively. (For interpretation of the references to color in this figure legend, the reader is referred to the web version of this article.)

discharge (panel a2). Remarkably, the location of the primary EMPM exhibits a critical point (jump) regarding the river flow (panel a3). This critical point can be clearly observed between $15\,m^3s^{-1}$ and $20\,m^3s^{-1}$. The location of the primary EMPM is shifted seaward from about km 30 to the mouth. It is worth noting that the order of magnitude of these discharges from the Alcalá del Río dam, although low, is usual in the GRE. Even within low river flow conditions ($Q<40\,m^3s^{-1}$), there is a notable variability in the location of the EMPM. The EMPM occur within the limits of the Natura 2000 protection area for all cases.

Fig. 7 shows the modeling results regarding the sensitivity of the MPs distribution patterns to the type of particles. Simulations are performed at the same mean environmental conditions that occurred during the field campaign. On the one hand, under those conditions, MP items with higher terminal velocities, i.e., higher buoyancy, are expected to be more easily trapped inside the estuary. This is evidenced by a greater difference between the MPC at the primary EMPM inside the estuary and

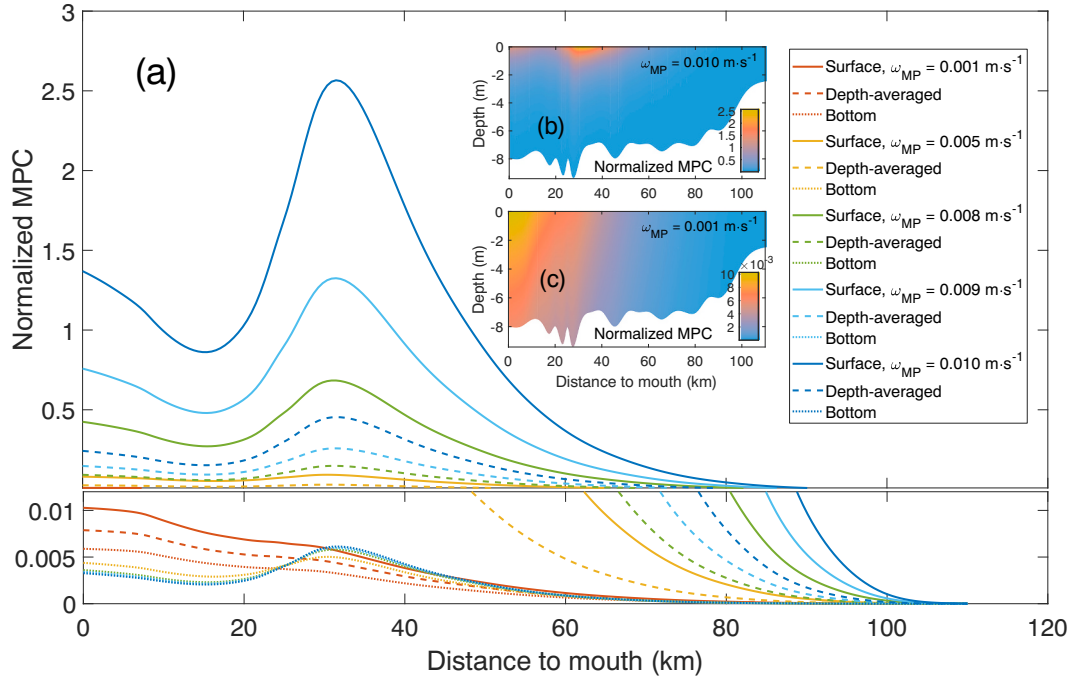

Fig. 7. Surface (solid curves), bottom (dotted), and depth-averaged (dashed) normalized MPC along the main channel of the estuary for different rising velocities, viz. ω_{MP}=0.001 $m\,s^{-1}$ (red curves), 0.005 $m\,s^{-1}$ (yellow), 0.008 $m\,s^{-1}$ (green), 0.009 $m\,s^{-1}$ (light blue), and 0.010 $m\,s^{-1}$ (dark blue). Insets (b) and (c) show color plots of normalized MPC for the ω_{MP}=0.010 $m\,s^{-1}$ and ω_{MP}=0.001 $m\,s^{-1}$ cases, respectively. Vertical axis has been split for clarity. (For interpretation of the references to color in this figure legend, the reader is referred to the web version of this article.)

that of the secondary EMPM near the mouth. For instance, MP particles with ω_{MP}=0.010 m s^{-1} concentrate significantly near km 30 (dark blue curves in panel a, and color plot in panel b). In addition, differences between bottom and surface concentrations are greater (solid vs. dotted curves). On the other hand, floating plastic particles with lower values of ω_{MP} (i.e., lower buoyancy due to lower relative density excess) are expected to be distributed more uniformly along the estuary (main graph, red curves) and flushed more easily out of the estuary. The lower the velocity ω_{MP}, for a given turbulent mixing level, the smaller the difference in concentration between surface (solid curves), bottom (solid curves) and depth-averaged (dashed curves) concentrations. This can also be observed in panel c (ω_{MP}=0.001 m s^{-1} case). Here, relatively high MPCs are observed near the bottom because this type of MPs is more easily dispersed by turbulence in the water column.

4. Conclusions

This study contributes to further understanding the relationships between MPs distribution and forcing in weakly stratified estuaries. Observations of MPs made on a monthly basis in the water column and modeling results in the Guadalquivir estuary were presented and analyzed. The aims were to quantify the along-estuary transport and identify potential hot-spots of MPs, as well as unravel the relative influence of the river discharge, density-driven, wind-driven, and tidal straining circulation on their spatio-temporal patterns. Answers to these research questions have been provided and translate into the following conclusions.

Similar mean number concentrations, viz. approx. 0.041 items m^{-3}, were found at the two stations analyzed, which were located in the lower and middle part of the estuary. Maximum monthly-averaged values of 0.15 items m^{-3} and 0.20 items m^{-3} were obtained at these stations, respectively. Although average values were much lower, peak MPCs were comparable to those reported in other estuarine areas. Differently from other water bodies, the highest MP fraction corresponded to polyethylene films (approx. 70%), followed by rigid fragments and lines, with lower numbers of foam or pellets. The predominance of films in the GRE might be related to the urban activity and, remarkably, to the intense agricultural activity developed in its catchment and margins. Diffuse water inputs from the margins in the middle part of the estuary could explain the positive relation between MPC values and local rainfall events, when there are no significant releases from the upstream dam.

Simulations were capable to reproduce and helped to explain the observed averaged MPCs at both stations during mean flow conditions. Modeling results reveal that the dominant contributions driving the net circulation depend on the particular location within the estuary, being the most significant among those considered in this study the tidal straining, density-driven flow, and river flow. River flow-induced circulation dominates the upper and middle parts of the estuary, tidal straining takes over the control in the lower stretches, and the density-driven flow dominates near the mouth. The convergence of transports associated with these contributions favors the trapping of MPs within the estuary in the stretch between the two sampling Stations at around km 25 from the estuary mouth. This (primary) Estuarine MP Maximum (EMPM) is located in the vicinity of the Doñana National Park – Natura 2000 protection area, and coincides with the location of one of the Estuarine Turbidity Maxima (ETM) of the Guadalquivir estuary.

CRediT authorship contribution statement

María Bermúdez: Methodology, Software, Validation, Formal analysis, Investigation, Writing – original draft, Writing – review & editing, Visualization. **César Vilas:** Methodology, Investigation, Resources, Data curation, Writing – review & editing, Funding acquisition. **Rocío Quintana:** Methodology, Formal analysis, Investigation, Data curation, Writing – review & editing. **Daniel González-Fernández:** Methodology, Formal analysis, Investigation, Data curation, Writing – review & editing. **Andrés Cózar:** Methodology, Formal analysis, Investigation, Resources, Data curation, Writing – review & editing. **Manuel Díez-Minguito:** Conceptualization, Software, Formal analysis, Investigation, Writing – original draft, Writing – review & editing, Funding acquisition.

Declaration of competing interest

The authors declare that they have no known competing financial interests or personal relationships that could have appeared to influence the work reported in this paper.

Acknowledgements

This research is funded by Spanish Ministry of Science, Innovation and Universities (AEI/FEDER/UE) through the projects CTM2016-77106-R and CTM2017-89531-R. Guadalquivir-LTER project was supported by IFAPA Research Projects PP.FEM.PPA201700.5 and PP.FEM.PP201900.5, 75% cofounded by European Maritime and Fisheries Fund (2014–2022), within the Spanish Operational Program "Fisheries and Maritime 2014–2020". MB and DGF acknowledge funding from the European Union's Horizon 2020 research and innovation programme under the Marie Skłodowska-Curie, grant agreements 754446 (UGR Research and Knowledge Transfer Fund – Athenea3i) and 846843 (LitRivus), respectively. University of Granada / CBUA provided the funding for open access charges. Finally, the authors would like to thank the two anonymous reviewers and Editor for their valuable comments and suggestions.

Appendix A. Supplementary data

Supplementary data to this article can be found online at https://doi.org/10.1016/j.marpolbul.2021.112622.

References

Barbier, E.B., Hacker, S.D., Kennedy, C., Koch, E.W., Stier, A.C., Silliman, B.R., 2011. The Value of Estuarine and Coastal Ecosystem Services, vol. 81. John Wiley & Sons, Ltd. https://doi.org/10.1890/10-1510.1

Borrelle, S.B., Ringma, J., Law, K.L., Monnahan, C.C., Lebreton, L., McGivern, A., Murphy, E., Jambeck, J., Leonard, G.H., Hilleary, M.A., et al., 2020. Predicted growth in plastic waste exceeds efforts to mitigate plastic pollution. Science 369, 1515–1518. https://doi.org/10.1126/science.aba3656.

Bowden, K.F., Fairbairn, L.A., Hughes, P., 1959. The distribution of shearing stresses in a tidal current. Geophys. J. R. Astron. Soc. 2, 288–305. https://doi.org/10.1111/j.1365-246X.1959.tb05801.x.

Burchard, H., Hetland, R.D., 2010. Quantifying the contributions of tidal straining and gravitational circulation to residual circulation in periodically stratified tidal estuaries. J. Phys. Oceanogr. 40, 1243–1262. https://doi.org/10.1175/2010JPO4270.1.

Caballero, I., Morris, E.P., Ruiz, J., Navarro, G., 2014. Assessment of suspended solids in the Guadalquivir estuary using new DEIMOS-1 medium spatial resolution imagery. Remote Sens. Environ. 146, 148–158. https://doi.org/10.1016/j.rse.2013.08.047.

Cañavate, J.P., van Bergeijk, S., Giráldez, I., González-Ortegón, E., Vílas, C., 2019. Fatty acids to quantify phytoplankton functional groups and their spatiotemporal dynamics in a highly turbid estuary. Estuar. Coasts 42, 1971–1990. https://doi.org/10.1007/s12237-019-00629-8.

Cañavate, J.P., van Bergeijk, S., González-Ortegón, E., Vílas, C., 2021. Contrasting fatty acids with other indicators to assess nutritional status of suspended particulate organic matter in a turbid estuary. Estuar. Coast. Shelf Sci. 254. https://doi.org/10.1016/j.ecss.2021.107329.

Chubarenko, I., Esiukova, E., Bagaev, A., Isachenko, I., Demchenko, N., Zobkov, M., Efimova, I., Bagaeva, M., Khatmullina, L., 2018. Behavior of Microplastics in Coastal Zones. Elsevier Inc. https://doi.org/10.1016/B978-0-12-813747-5.00006-0

Cobos, M., Baquerizo, A., Díez-Minguito, M., Losada, M.A., 2020. A subtidal box model based on the longitudinal anomaly of potential energy for narrow estuaries. An application to the Guadalquivir River Estuary (SW Spain). J. Geophys. Res. Oceans 125, 1–19. https://doi.org/10.1029/2019JC015242.

Cohen, J.H., Internicola, A.M., Mason, R.A., Kukulka, T., 2019. Observations and simulations of microplastic debris in a tide, wind, and freshwater-driven estuarine environment: the Delaware Bay. Environ. Sci. Technol. 53, 14204–14211. https://doi.org/10.1021/acs.est.9b04814.

Cózar, A., Echevarra, F., González-Gordillo, J.I., Irigoien, X., Úbeda, B., Hernández-León, S., Palma, Á.T., Navarro, S., García-de Lomas, J., Ruiz, A., et al., 2014. Plastic debris in the open ocean. Proc. Natl. Acad. Sci. 111, 10239–10244.

Cózar, A., Sanz-Martín, M., Martí, E., González-Gordillo, J.I., Ubeda, B., Gálvez, J.Á., Irigoien, X., Duarte, C.M., 2015. Plastic accumulation in the Mediterranean Sea. PLoS ONE 10, e0121762. https://doi.org/10.1371/journal.pone.0121762.

Cózar, A., Martí, E., Duarte, C.M., García-de Lomas, J., Van Sebille, E., Ballatore, T.J., Eguíluz, V.M., Ignacio González-Gordillo, J., Pedrotti, M.L., Echevarría, F., Troublè, R., Irigoien, X., 2017. The Arctic Ocean as a dead end for floating plastics in the North Atlantic branch of the Thermohaline Circulation. Sci. Adv. 3, 1–9. https://doi.org/10.1126/sciadv.1600582.

de Carvalho-Souza, G.F., González-Ortegón, E., Baldó, F., Vilas, C., Drake, P., Llope, M., 2019. Natural and anthropogenic effects on the early life stages of European anchovy in one of its essential fish habitats, the Guadalquivir estuary. Mar. Ecol. Prog. Ser. 617, 67–79. https://doi.org/10.3354/meps12562.

Díez-Minguito, M., de Swart, H.E., 2018. Observational Evidences of Strain-induced Periodic Stratification (SIPS) in the Guadalquivir Estuary. V Encuentro de Oceanografía Física 2018 (EOF), Vigo (Spain), pp. 124–125.

Díez-Minguito, M., de Swart, H.E., 2020. Relationships between chlorophyll-a and suspended sediment concentration in a high-nutrient load estuary: an observational and idealized modeling approach. J. Geophys. Res. Oceans 125. https://doi.org/10.1029/2019JC015188.

Díez-Minguito, M., Baquerizo, A., Ortega-Sánchez, M., Navarro, G., Losada, M.A., 2012. Tide transformation in the Guadalquivir estuary (SW Spain) and process-based zonation. J. Geophys. Res. Oceans 117 (C3), 1–14. https://doi.org/10.1029/2011JC007344.

Díez-Minguito, M., Contreras, E., Polo, M.J., Losada, M.A., 2013. Spatio-temporal distribution, along-channel transport, and post-riverflood recovery of salinity in the Guadalquivir estuary (SW Spain). J. Geophys. Res. Oceans 118, 2267–2278. https://doi.org/10.1002/jgrc.20172.

Díez-Minguito, M., Baquerizo, A., de Swart, H.E., Losada, M.A., 2014. Structure of the turbidity field in the Guadalquivir estuary: analysis of observations and a box model approach. J. Geophys. Res. Oceans 119, 7190–7204. https://doi.org/10.1002/2014JC010210.

Díez-Minguito, M., Bermúdez, M., Gago, J., Carretero, O., Viñas, L., 2020. Observations and idealized modelling of microplastic transport in estuaries: the exemplary case of an upwelling system (Ría de Vigo, NW Spain). Mar. Chem. 222, 103780. https://doi.org/10.1016/j.marchem.2020.103780.

González-Fernández, D., Cózar, A., Hanke, G., Viejo, J., Morales-Caselles, C., Bakiu, R., Barceló, D., Bessa, F., Bruge, A., Cabrera, M., Castro-Jiménez, J., Constant, M., Crosti, R., Galletti, Y., Kideys, A.E., Machitadze, N., Pereira de Brito, J., Pogojeva, M., Ratola, N., Rigueira, J., Rojo-Nieto, E., Savenko, O., Schöneich-Argent, R.I., Siedlewicz, G., Suaria, G., Tourgeli, M., 2021. Floating macro-litter leaked from Europe to the ocean. Nat. Sustain. 4, 474–483. https://doi.org/10.1038/s41893-021-00722-6.

González-Ortegón, E., Subida, M.D., Arias, A.M., Baldó, F., Cuesta, J.A., Fernández-Delgado, C., Vilas, C., Drake, P., 2012. Nekton response to freshwater inputs in a temperate European Estuary with regulated riverine inflow. Sci. Total Environ. 440, 261–271. https://doi.org/10.1016/j.scitotenv.2012.06.061.

González-Ortegón, E., Baldó, F., Arias, A., Cuesta, J.A., Fernández-Delgado, C., Vilas, C., Drake, P., 2015. Freshwater scarcity effects on the aquatic macrofauna of a European Mediterranean-climate estuary. Sci. Total Environ. 503–504, 213–221. https://doi.org/10.1016/j.scitotenv.2014.06.020.

González-Ortegón, E., de los Ríos, I., Sparaventi, E., Baldo, F., Sanchez, R., Sendra, M., Yeste, M., 2020. Microplastic pollution in the surface waters of the Gulf of Cadiz. In: VII International Conference of Marine Sciences. Workshop on Marine Litter, p. 34.

Gray, A.D., Wertz, H., Leads, R.R., Weinstein, J.E., 2018. Microplastic in two South Carolina Estuaries: occurrence, distribution, and composition. Mar. Pollut. Bull. 128, 223–233. https://doi.org/10.1016/j.marpolbul.2018.01.030.

Jalón-Rojas, I., Wang, X.H., Fredj, E., 2019. A 3D numerical model to Track Marine Plastic Debris (TrackMPD): sensitivity of microplastic trajectories and fates to particle dynamical properties and physical processes. Mar. Pollut. Bull. 141, 256–272. https://doi.org/10.1016/j.marpolbul.2019.02.052.

Kane, I.A., Clare, M.A., 2019. Dispersion, accumulation, and the ultimate fate of microplastics in deep-marine environments: a review and future directions. Front. Earth Sci. 7 https://doi.org/10.3389/feart.2019.00080.

Lebreton, L.C., Van der Zwet, J., Damsteeg, J.W., Slat, B., Andrady, A., Reisser, J., 2017. River plastic emissions to the world's oceans. Nat. Commun. 8 https://doi.org/10.1038/ncomms15611.

Lindeque, P.K., Cole, M., Coppock, R.L., Lewis, C.N., Miller, R.Z., Watts, A.J., Wilson-McNeal, A., Wright, S.L., Galloway, T.S., 2020. Are we underestimating microplastic abundance in the marine environment? A comparison of microplastic capture with nets of different mesh-size. Environ. Pollut. 265, 114721. https://doi.org/10.1016/j.envpol.2020.114721.

Llope, M., 2017. The ecosystem approach in the Gulf of Cadiz. A perspective from the southernmost European Atlantic regional sea. ICES J. Mar. Sci. 74, 382–390. https://doi.org/10.1093/icesjms/fsw165.

López-López, J.A., García-Vargas, M., Moreno, C., 2011. A chemometric approach to the evaluation of atmospheric and fluvial pollutant inputs in aquatic systems: the Guadalquivir River estuary as a case study. Environ. Pollut. 159, 1136–1143. https://doi.org/10.1016/j.envpol.2011.02.006.

Mai, L., You, S.N., He, H., Bao, L.J., Liu, L.Y., Zeng, E.Y., 2019. Riverine microplastic pollution in the Pearl River Delta, China: are modeled estimates accurate? Environ. Sci. Technol. 53, 11810–11817. https://doi.org/10.1021/acs.est.9b04838.

Martí, E., Martin, C., Galli, M., Echevarría, F., Duarte, C.M., Cózar, A., 2020. The colors of the ocean plastics. Environ. Sci. Technol. 54, 6594–6601. https://doi.org/10.1021/acs.est.9b06400.

Miró, J.M., Megina, C., Donázar-Aramendía, I., Reyes-Martínez, M.J., Sánchez-Moyano, J.E., García-Gómez, J.C., 2020. Environmental factors affecting the nursery function for fish in the main estuaries of the Gulf of Cadiz (south-west Iberian Peninsula). Sci. Total Environ. 737 https://doi.org/10.1016/j.scitotenv.2020.139614.

Morales-Caselles, C., Viejo, J., Martí, E., González-Fernández, D., Pragnell-Raasch, H., González-Gordillo, J.I., Montero, E., Arroyo, G.M., Hanke, G., Salvo, V., Basurko, O. C., Mallos, N., Lebreton, L., Echevarría, F., van Emmerik, T., Duarte, C.M., Gálvez, J. A., van Sebille, E., Galgani, F., García, C.M., Ross, P.S., Bartual, A., Ioakeimidis, C., Markalain, G., Isobe, A., Cózar, A., 2021. An inshore-offshore sorting system revealed from global classification of ocean litter. Nat. Sustain. 4, 484–493. https://doi.org/10.1038/s41893-021-00720-8.

Naidoo, T., Glassom, D., Smit, A.J., 2015. Plastic pollution in five urban estuaries of KwaZulu-Natal, South Africa. Mar. Pollut. Bull. 101, 473–480. https://doi.org/10.1016/j.marpolbul.2015.09.044.

Navarro, G., Gutiérrez, F.J., Díez-Minguito, M., Losada, M.A., Ruiz, J., 2011. Temporal and spatial variability in the Guadalquivir estuary: a challenge for real-time telemetry. Ocean Dyn. 61, 753–765. https://doi.org/10.1007/s10236-011-0379-6.

Piehl, S., Leibner, A., Löder, M.G., Dris, R., Bogner, C., Laforsch, C., 2018. Identification and quantification of macro- and microplastics on an agricultural farmland. Sci. Rep. 8, 17950. https://doi.org/10.1038/s41598-018-36172-y.

Prata, J.C., Godoy, V., da Costa, J.P., Calero, M., Martín-Lara, M.A., Duarte, A.C., Rocha-Santos, T., 2021. Microplastics and fibers from three areas under different anthropogenic pressures in Douro river. Sci. Total Environ. 776, 145999. https://doi.org/10.1016/j.scitotenv.2021.145999.

Prieto, L., Navarro, G., Rodríguez-Gálvez, S., Huertas, I.E., Naranjo, J.M., Ruiz, J., 2009. Oceanographic and meteorological forcing of the pelagic ecosystem on the Gulf of Cadiz shelf (SW Iberian Peninsula). Cont. Shelf Res. 29, 2122–2137. https://doi.org/10.1016/j.csr.2009.08.007.

Quintana, R., González, D., Cózar, A., Vilas, C., González-Ortegón, E., Baldo, F., Morales, C., 2020. Plastic waste input from Guadalquivir River to the ocean. In: EGU General Assembly Conference Abstracts, p. 19268.

Reyes-Merlo, M.Á., Díez-Minguito, M., Ortega-Sánchez, M., Baquerizo, A., Losada, M.Á., 2013. On the relative influence of climate forcing agents on the saline intrusion in a well-mixed estuary: medium-term Monte Carlo predictions. J. Coast. Res. 165, 1200–1205. https://doi.org/10.2112/si65-203.1.

Rochman, C.M., Brookson, C., Bikker, J., Djuric, N., Earn, A., Bucci, K., Athey, S., Huntington, A., McIlwraith, H., Munno, K., Frond, H.D., Kolomijeca, A., Erdle, L., Grbic, J., Bayoumi, M., Borrelle, S.B., Wu, T., Santoro, S., Werbowski, L.M., Zhu, X., Giles, R.K., Hamilton, B.M., Thaysen, C., Kaura, A., Klasios, N., Ead, L., Kim, J., Sherlock, C., Ho, A., Hung, C., 2019. Rethinking microplastics as a diverse contaminant suite. Environ. Toxicol. Chem. 38, 703–711. https://doi.org/10.1002/etc.4371.

Roebroek, C.T., Harrigan, S., Van Emmerik, T.H., Baugh, C., Eilander, D., Prudhomme, C., Pappenberger, F., 2021. Plastic in global rivers: are floods making it worse? Environ. Res. Lett. 16, 025003. https://doi.org/10.21203/rs.3.rs-43330/v1.

Ruiz, J., Polo, M.ª., Díez-Minguito, M., Navarro, G., Morris, E.P., Huertas, E., Caballero, I., Contreras, E., Losada, M.A., 2015. The Guadalquivir Estuary: A Hot Spot for Environmental and Human Conflicts, p. vol. 8. https://doi.org/10.1007/978-3-319-06305-8_8.

Ruiz, J., Macías, D., Navarro, G., 2017. Natural forcings on a transformed territory overshoot thresholds of primary productivity in the Guadalquivir estuary. Cont. Shelf Res. 148, 199–207. https://doi.org/10.1016/j.csr.2017.09.002.

Ryan, P.G., Perold, V., 2021. Limited dispersal of riverine litter onto nearby beaches during rainfall events. Estuar. Coast. Shelf Sci. 251, 107186. https://doi.org/10.1016/j.ecss.2021.107186.

Simon-Sánchez, L., Grelaud, M., Garcia-Orellana, J., Ziveri, P., 2019. River Deltas as hotspots of microplastic accumulation: the case study of the Ebro River (NW Mediterranean). Sci. Total Environ. 687, 1186–1196. https://doi.org/10.1016/j.scitotenv.2019.06.168.

Sousa, M.C., DeCastro, M., Gago, J., Ribeiro, A.S., Des, M., Gómez-Gesteira, J.L., Dias, J. M., Gomez-Gesteira, M., 2021. Modelling the distribution of microplastics released by wastewater treatment plants in Ria de Vigo (NW Iberian Peninsula). Mar. Pollut. Bull. 166 https://doi.org/10.1016/j.marpolbul.2021.112227.

Talke, S.A., de Swart, H.E., Schuttelaars, H.M., 2009. Feedback between residual circulations and sediment distribution in highly turbid estuaries: an analytical model. Cont. Shelf Res. 29, 119–135. https://doi.org/10.1016/j.csr.2007.09.002.

Waldschläger, K., Born, M., Cowger, W., Gray, A., Schüttrumpf, H., 2020. Settling and rising velocities of environmentally weathered micro- and macroplastic particles. Environ. Res. 191. https://doi.org/10.1016/j.envres.2020.110192.

Weithmann, N., Möller, J.N., Löder, M.G., Piehl, S., Laforsch, C., Freitag, R., 2018. Organic fertilizer as a vehicle for the entry of microplastic into the environment. Sci. Adv. 4, eaap8060 https://doi.org/10.1126/sciadv.aap8060.

Windsor, F.M., Durance, I., Horton, A.A., Thompson, R.C., Tyler, C.R., Ormerod, S.J., 2019. A Catchment-Scale Perspective of Plastic Pollution. https://doi.org/10.1111/gcb.14572.

Wright, S.L., Kelly, F.J., 2017. Plastic and human health: a micro issue? Environ. Sci. Technol. 51, 6634–6647. https://doi.org/10.1021/acs.est.7b00423.

Wright, S.L., Thompson, R.C., Galloway, T.S., 2013. The Physical Impacts of Microplastics on Marine Organisms: A Review. https://doi.org/10.1016/j.envpol.2013.02.031.

WWF, 2019. Doñana bajo plástico: Avanza la invasión de los frutos rojos. URL: https://wwfes.awsassets.panda.org/downloads/donana_bajo_plastico.pdf?51960/Donana-bajo-plastico-avanza-la-invasion-de-los-frutos-rojos.

Yonkos, L.T., Friedel, E.A., Perez-Reyes, A.C., Ghosal, S., Arthur, C.D., 2014. Microplastics in four estuarine rivers in the Chesapeake bay, U.S.A. Environ. Sci. Technol. 48, 14195–14202. https://doi.org/10.1021/es5036317.